Journal of Solid State Chemistry 200 (2013) 265–270

Contents lists available at SciVerse ScienceDirect

Journal of Solid State Chemistry

journal homepage: www.elsevier.com/locate/jssc

Topological evolution and photoluminescent properties of a series of divalent zinc-based metal–organic frameworks tuned via ancillary ligating spacers

Xiao-Min Lian, Wen Zhao, Xiao-Li Zhao *

Shanghai Key Laboratory of Green Chemistry and Chemical Processes, Department of Chemistry, East China Normal University, 3663 North Zhongshan Road, Shanghai 200062, PR China

ARTICLE INFO

Article history:
Received 19 October 2012
Received in revised form
4 January 2013
Accepted 6 January 2013
Available online 31 January 2013

Keywords:
Acylamide functionality
MOF
Bipyridine
4-(4-carboxybenzamido)benzoic acid
Photoluminescent property

ABSTRACT

The combination of divalent zinc ions, 4-(4-carboxybenzamido)benzoic acid and exo-bidendate bipyridine ligands gave rise to a series of new MOFs: $[ZnL(bipy)]\cdot DMF\cdot H_2O$ (**1**), $[ZnL(bpe)]\cdot 1.5H_2O$ (**2**), $[ZnL(bpa)]\cdot 4H_2O$ (**3**) and $[ZnL(bpp)]\cdot 1.75H_2O$ (**4**) (MOF=metal-organic framework, bipy=4,4′-bipyridine, bpe=*trans*-1,2-bis(4-pyridyl)ethylene, bpa=1,2-bis(4-pyridinyl)ethane, bpp=1,3-bis(4-pyridinyl)propane, H_2L=4,4′-(carbonylimino)dibenzoic acid). Fine tune over the topology of the MOFs was achieved via systematically varying the geometric length of the second ligating bipyridine ligands. Single-crystal X-ray analysis reveals that complex **1** has a triply interpenetrated three-dimensional (3D) framework with elongated primitive cubic topology, whereas isostructural complexes **2** and **3** each possesses a 6-fold interpenetrated diamondiod 3D framework. Further expansion of the length of the bipyridine ligand to bpp leads to the formation of **4**, which features an interesting entangled architecture of 2D→3D parallel polycatenation. In addition, the thermogravimetric analyses and solid-state photoluminescent properties of the selected complexes are investigated.

1. Introduction

Intense interest in the chemistry of metal-organic frameworks (MOFs) stems from their topological aesthetics and intriguing potential applications as new functional solid materials for gas storage, separation, heterogeneous catalysis, etc [1]. Most of these applications are highly associated with the porosity of MOFs. One of the main concerns regarding porosity of MOFs is catenation, which will mitigate the free volume and reduce the pore size. Nevertheless, the existence of catenation is not always negative, as their occurrence will contribute much to the structural diversity and intrigue of MOFs [2]. Moreover, catenation can lead to materials with enhanced properties or functions, such as superhard materials [3], magnetic materials [4], and materials with high stability or enhanced adsorption capacity [5]. A conventional strategy of using long exo-multidentate ligands has been successful to construct polycatenated networks. Recently, a handful of new protocols such as liquid-phase epitaxial growth, templated synthesis, manipulation of reaction conditions have been applied to manipulate the catenation behavior of MOFs and thus improve their properties [6]. In this report, we address tune of catenation by incorporation of the exo-bidentate bipyridine ligands 4,4′-bipyridine (bipy), *trans*-1,2-bis(4-pyridyl)ethylene (bpe), 1,2-bis(4-pyridinyl)ethane (bpa), 1,3-bis(4-pyridinyl)propane (bpp) into the Zn^{2+}–H_2L system, anticipating that systematic investigation of the effects of the pyridyl-based spacer ligands on the formation of MOFs will be explored. The synthetic strategy takes advantage of four factors: (1) the combination of multicarboxylate ligands and multipyridyl ligands incorporates the virtues of different functional groups to control the resulting architecture by changing one of the ligands [7]; (2) the acylamide group possesses both hydrogen-bonding donor and acceptor sites and has been extensively employed in the construction of MOFs with guest-accessible functional organic sites for catalysis inside the channels [8]; (3) both theoretical studies and experimental observations indicate that decoration of MOFs with polar acylamide groups can significantly enhance the CO_2 binding ability and selectivity of MOFs. This will improve their properties for practical applications such as natural gas purification and greenhouse gas control [9]. (4) It is well documented that exo-bidendate nitrogen ligands such as bipy, bpe, bpa and bpp can coordinate to metal ions as spacer ligands [10]. Execution of the synthetic procedure shown in Scheme 1 yielded the following four complexes, $[ZnL(bipy)]\cdot DMF\cdot H_2O$ (**1**), $[ZnL(bpe)]\cdot 1.5H_2O$ (**2**), $[ZnL(bpa)]\cdot 4H_2O$ (**3**) and $[ZnL(bpp)]\cdot 1.75H_2O$ (**4**), whose structures and photoluminescent properties will be presented.

2. Experimental

2.1. Materials and physical measurements

All chemicals and reagents of analytical grade were commercially available and used without further purification. 4,4′-(carbonylimino)dibenzoic acid (H_2L) was synthesized according to

* Corresponding author. Fax: +86 21 62233179.
E-mail address: xlzhao@chem.ecnu.edu.cn (X.-L. Zhao).

0022-4596/$ - see front matter © 2013 Elsevier Inc. All rights reserved.
http://dx.doi.org/10.1016/j.jssc.2013.01.004

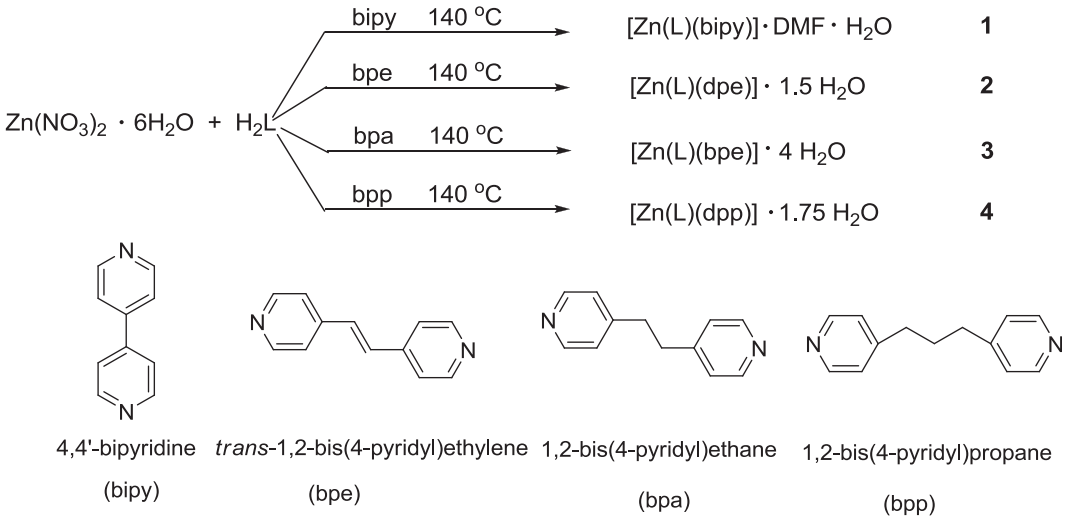

Scheme 1.

the reported methods [11]. NMR spectra were obtained using a Bruker Avance III 400M instrument. Elemental analyses were determined on a Vario ELIII Elemental Analyzer. The IR spectra were recorded on a Bruker TENSOR 27 spectrometer in the 4000–500 cm^{-1} range. Thermogravimetric analyses (TGA) were carried out on a Netzsch STA 449 F3 instrument with a heating rate of 10 °C min^{-1} under N_2 atmosphere. Powder X-ray diffraction (PXRD) data were recorded using a Rigaku (D/Max-Ultima IV) diffractometer equipped with Cu-$K\alpha$ radiation, with a step size and a scan speed of 0.02° min^{-1} and 5° min^{-1}, respectively. Simulated PXRD patterns were calculated with the Mercury program using the single crystal data [12]. Solid-state photoluminescent spectra of complexes **1–4** were measured on a Varian Cary Eclipse fluorescence spectrometer.

2.2. Synthesis of [ZnL(bipy)]·DMF·H_2O (1)

A mixture of H_2L (20.00 mg, 0.07 mmol), bipy (10.93 mg, 0.07 mmol) and $Zn(NO_3)_2 \cdot 6H_2O$ (20.86 mg, 0.07 mmol) in 4 mL DMF/H_2O (1:7) was placed in a 15 mL Teflon-lined autoclave and subjected to solvothermal condition at 140 °C for 48 h after ultrasonic treatment and then cooled to room temperature (cooling rate 0.1 °C min^{-1}). Colorless needle-shaped crystals were collected by filtration and washed with DMF to give **1** (32 mg, yield: 77% based on H_2L). Anal. Calcd for $C_{28}H_{26}ZnN_4O_7$ (M_r=595.91): C, 56.43; H, 4.40; N, 9.40. Found: C, 56.41; H, 4.27; N, 9.46. IR: 3482(w), 3074(w), 1662(s), 1604(s), 1541(s), 1396(vs), 1322(s), 1258(m), 1220(w), 1179(m), 1148(m), 1098(s), 1069(m), 1046(m), 1017(s), 860(s), 820(vs), 783(vs), 729(vs), 632(m), 609(s).

2.3. Synthesis of [ZnL(bpe)]·1.5H_2O (2)

Complex **2** was synthesized in a similar manner to **1** except that bpe was used instead of bipy. Colorless block-like crystals were isolated in 84% yield (based on H_2L). IR: 3481(w), 2990(w), 1655(w), 1613(vs), 1524(m), 1509(m), 1432(w), 1373(vs), 1318(s), 1254(s), 1175(w), 1140(m), 1099(w), 1069(w), 1027(s), 977(m), 860(w), 837(s), 812(w), 778(s), 729(s), 657(w).

2.4. Synthesis of [ZnL(bpa)]·4H_2O (3)

When the procedure for **1** was repeated using bpa instead of bipy, colorless block-like crystals of **3** were obtained in 78% yield (based on H_2L). IR: 3446(w), 2928(w), 1660(vs), 1604(vs), 1561(w), 1526(s), 1431(w), 1381(vs), 1321(s), 1255(s), 1175(m), 1141(w), 1099(m), 1069(m), 1030(m), 1018(m), 900(w), 861(s), 833(s), 816(s), 783(s), 733(s), 701(m), 663(m).

2.5. Synthesis of [ZnL(bpp)]·1.75H_2O (4)

The synthetic procedure of **1**was repeated using bpp instead of bipy. Colorless block-like crystals were obtained in 69% yield (based on H_2L). Anal. Calcd for $C_{28}H_{26.5}ZnN_3O_{6.75}$ (M_r=578): C, 58.14; H, 4.62; N, 7.26. Found: C, 57.96; H, 4.82; N, 7.16. IR: 3444(w), 1943(m), 1613(vs), 1529(s), 1434(w), 1368(vs), 1322(s), 1255(m), 1177(m), 1140(m), 1070(m), 1031(m), 1017(m), 900(w), 880(w), 858(m), 812(m), 784(s), 733(s), 701(w), 656(w), 626(w).

2.6. X-ray crystallography

Selected crystals were used for data-collection on a Bruker SMART ApexII diffractometer equipped with graphite-monochromatic Mo $K\alpha$ radiation (λ=0.71073 Å) at 173 K cooled in a nitrogen stream. Frames were collected at 0.5° intervals in φ and ω for 30 s per frame such that a hemisphere of data was collected. Raw data collection and refinement were done using SMART. Data reduction was performed using SAINT+. Absorption corrections were applied using the SADABS program. For **1**, the structure was solved by Patterson method. For **2**, **3** and **4**, the structures were solved by direct method. All the structures were then refined by full-matrix least-squares on F^2 with anisotropic displacement using SHELX-97 [13]. Non-hydrogen atoms were refined with anisotropic displacement parameters during the final cycles. All the hydrogen atoms attached to carbon atoms were placed in calculated positions and refined using the riding model. Potential solvent accessible area and void space were calculated using the PLATON/SOLV [14]. For **1**, the uncoordinated DMF molecules are disordered and were treated using the split-atom models. The coordinated L^{2-} in **2** was treated using the split-atom models with half occupancies for each set to obtain the appropriate thermal parameters. Crystal data and structure refinement details are summarized in Table 1.

3. Results and discussions

3.1. Structural description of [ZnL(bipy)]·DMF·H_2O (1)

Solvothermal reaction of H_2L with $Zn(NO_3)_2 \cdot 6H_2O$ and bipy in DMF–H_2O system resulted in the formation of complex **1**. Single-crystal structure analysis reveals that **1** crystallize in monoclinic space group $P2_1/c$. The asymmetric unit of **1** contains one Zn^{II} atom, one bipy, one L^{2-}, one uncoordinated DMF and one lattice water molecule. As shown in Fig. 1a, Zn^{II} adopts a slightly distorted octahedral geometry, being coordinated by four carboxylate oxygen atoms from three L^{2-} ligands (the Zn–O distances are in the ranges of 2.038(3) Å and 2.277(3) Å) and two nitrogen atoms from two bipy molecules (Zn1–N1 = 2.132(3) Å, Zn1–N2 = 2.140(3) Å). Four carboxylate groups from four symmetry-related L^{2-} ligands coordinate to two Zn^{II} centers to form the dinuclear $Zn_2(COO)_4$ secondary building unit (SBU), which are further bridged by L^{2-} to form a (4,4) rhomboid grid layer. Within each layer, the rhomboid windows have dimensions of 19.02 Å × 19.02 Å with angles of 82.36° and 97.64° (defined by Zn···Zn distances and Zn···Zn···Zn angles) (Fig. 1b). Further pillaring of the layers through bipy ligands generates a 3D pillar-layer architecture, and the Zn/Zn distance through the bipy ligand is 11.35 Å (Fig. 1c). The topology of **1** can be best described as an elongated primitive cubic net. A 3-fold interpenetrating framework is observed due to the existence of large channels (Fig. 1c and d). The total accessible volume after removal of the guest DMA and water molecules is 26.9% using the PLATON/VOID routine.

3.2. Structural description of [ZnL(bpe)]·1.5H_2O (2) and [ZnL(bpa)]·4H_2O (3)

Further expansion of the length of the exo-bidendate bipyridine ligand to bpe and bpa leads to the formation of complexes **2** and **3**, respectively. X-ray analysis showed **2** and **3** are virtually isostructural though both crystallize in different space groups (for complex **2**, triclinic, $P\bar{1}$; for complex **3**, orthorhombic, *Pccn*). The following discussion on the structural aspect will mainly focus on complex **2**. Single-crystal X-ray analysis reveals that the asymmetric unit of crystal **2** consists of one Zn^{II}, two halves bpe and two halves L^{2-} ligands. Each Zn^{II} ion is in a slightly distorted tetrahedral geometry, being coordinated by two carboxylate oxygen atoms from two L^{2-} and two nitrogen atoms from two bpe molecules (for complex **2**, Fig. 2a; for complex **3**, Fig. 3a). The Zn–O and Zn–N bond lengths fall into the range of 1.930(5)–1.935(5) Å and 2.039 (5)–2.047 (4) Å, respectively. The Zn^{II} atom serves as node with L^{2-} and bpe ligands as linkers to construct a 3D structure with a diamondoid topology (for complex **2**, Fig. 2c; for complex **3**, Fig. 3c). A cavity with the pore 31 Å × 20 Å is generated by an independent equivalent diamondoid cage (for complex **2**, Fig. 2b; for complex **3**, Fig. 3b). The potential voids are large enough to generate a 6-fold interpenetrating 3D architecture with a diamondoid topology (for complex **2**, Fig. 2d; for complex **3**, Fig. 3d). It is noteworthy that only 15.8% of the effective free volume in the desolvated **2** is left due to the 6-fold interpenetration. For **3**, the pore void space is 25.8% after six-fold interpenetration. It is noteworthy that complex **3** still exhibits a 1D rectangle channels about 8.6 Å × 9.2 Å along the *b* axis despite the 6-fold interpenetration.

3.3. Structural description of [ZnL(bpp)]·1.75H_2O (4)

Continuous increase of the length and flexibility of the ancillary ligand was achieved when bpp was used instead of bpe and complex **4** with 2D → 3D parallel polycatenation architecture was harvested. Complex **4** crystallizes in monoclinic space group $P2_1/c$, the crystallographically independent Zn^{II} is four-coordinated in a tetrahedral geometry being coordinated by two carboxylate oxygen atoms and two pyridyl nitrogen atoms (Fig. 4a). Further extension of the $[ZnN_2O_2]$ tetrahedron through the bpp and L^{2-} form a 4-coordinated highly corrugated layer structure with 4^4-sql topology (Fig. 4b). The rhomboid voids with dimensions of 12 Å × 17 Å and angles of 97° and 90° (defined by Zn···Zn distance and Zn···Zn···Zn angles) within each layer allow interpenetration between adjacent layers to occur. The most intriguing feature of **4** is the 2D → 3D parallel polycatenation. The 4^4-sql layers stack with an ABAB sequences, and each of these equivalent layers is polycatenated with the adjacent two parallel layers (Fig. 4c). To the best of our knowledge, 2D → 3D parallel polycatenation based on 4^4-sql layers is rare and only few examples have been reported [15].

3.4. Thermal stability analysis and powder X-ray diffraction (PXRD) analysis

Thermogravimetric analyses (TGA) are performed on crystalline samples to examine the thermal stability (Figs. S1–S4). For **1**,

Table 1
Crystallographic data of complexes **1**–**4**.

Compound	**1**	**2**	**3**	**4**
Empirical Formula	$C_{28}H_{26}N_4O_7Zn$	$C_{27}H_{22}N_3O_{6.5}Zn$	$C_{27}H_{29}N_3O_9Zn$	$C_{28}H_{26.5}N_3O_{6.75}Zn$
M [g mol^{-1}]	595.87	557.86	604.91	578.41
Crystal system	Monoclinic	Triclinic	Orthorhombic	Monoclinic
Space group	$P2_1/c$	$P\bar{1}$ $\bar{1}$	*Pccn*	$P2_1/c$
a [Å]	9.6217(5)	8.3235(4)	23.2651(1)	9.4166(5)
b [Å]	28.6285(1)	11.6874(6)	15.2345(9)	25.7859(1)
c [Å]	10.4801(5)	13.3742(7)	16.8340(1)	11.9616(6)
α [°]	90	80.737(2)	90	90
β [¡]	111.3760(1)	85.828(2)	90	108.6140(1)
γ [¡]	90	83.364(2)	90	90
V [A^3]	2688.2(2)	1273.53(1)	5966.5(6)	2752.5(2)
Z	4	2	8	4
$\rho_{calcd.}$ [g cm^{-3}]	1.465	1.417	1.329	1.385
μ(Mo-$K\alpha$) [mm^{-1}]	0.968	1.008	0.876	0.941
F(0 0 0)	1220	556	2448	1180
θ range, °	2.20–25.01	1.55–25.00	2.00–25.01	1.96–25.01
R_{int}	0.0345	0.0248	0.0587	0.0317
Final R indices [$I > 2\sigma(I)$]	R_1 = 0.0563, wR_2 = 0.1221	R_1 = 0.0793, wR_2 = 0.2207	R_1 = 0.1275, wR_2 = 0.2552	R_1 = 0.0575, wR_2 = 0.1436
R indices (all data)	R_1 = 0.0607, wR_2 = 0.1238	R_1 = 0.0880, wR_2 = 0.2324	R_1 = 0.1475, wR_2 = 0.2726	R_1 = 0.0743, wR_2 = 0.1594

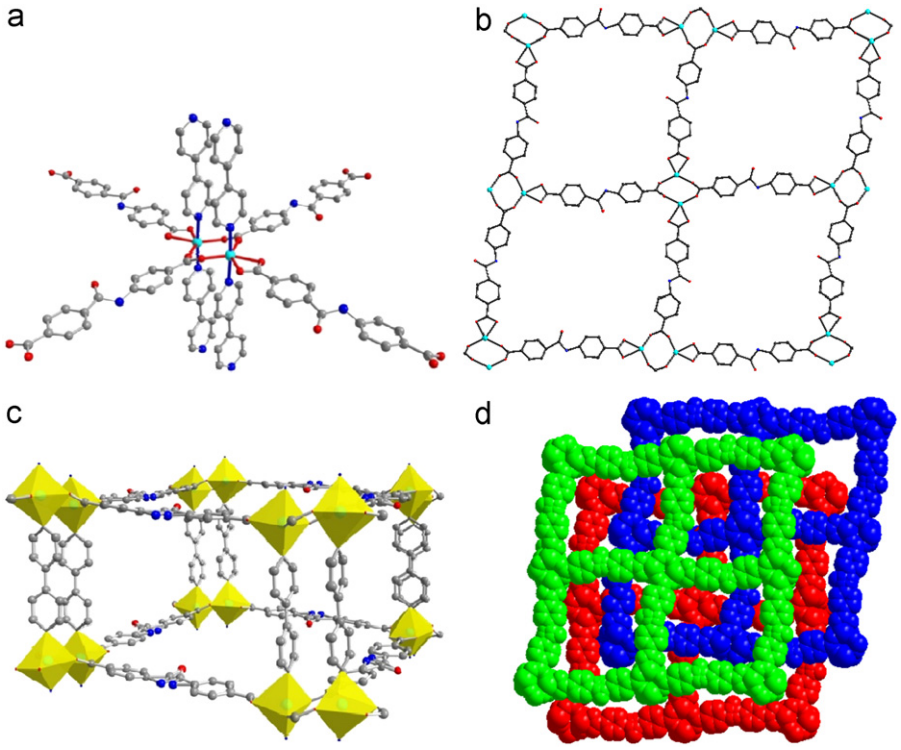

Fig. 1. Crystal structure of [ZnL(bipy)] · DMF · H_2O (**1**): (a) the coordination environment of Zn^{II} in **1**; (b) Single ZnL layer in **1**; (c) pillared 3D structure of **1**; (d) Space-filling showing of the 3-fold interpenetrating framework of **1**.

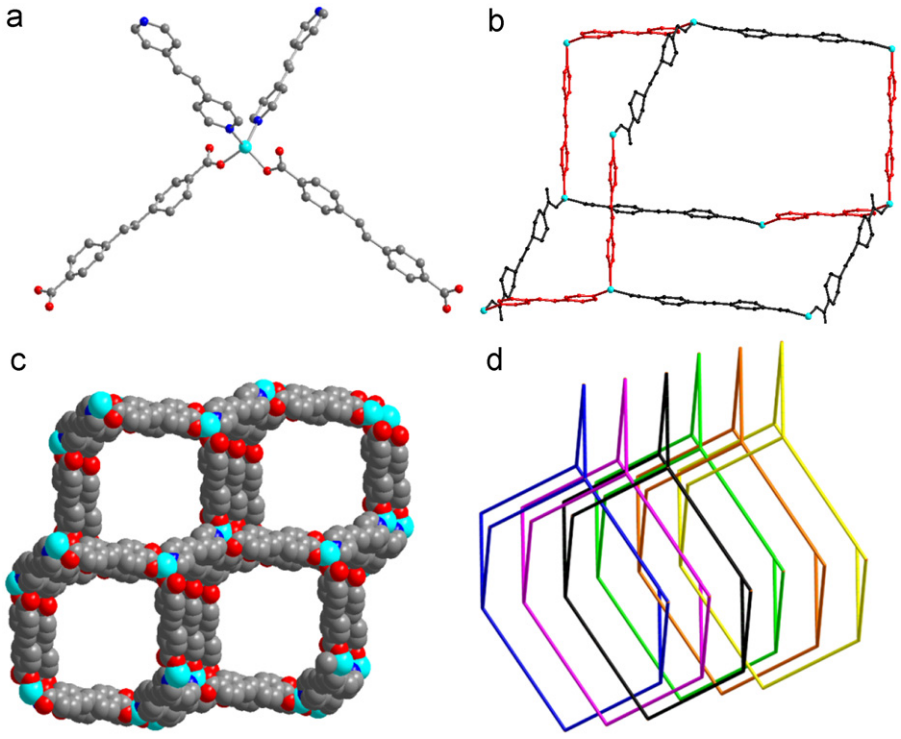

Fig. 2. Crystal structure of [ZnL(bpe)] · 1.5H_2O (**2**): (a) coordination environment around Zn^{II}; (b) the single diamondoid cage in **2**. Ligand bpe and L are represented in red and gray, respectively; (c) a single 3D framework of **2**; (d) schematic diagram of the 6-fold interpenetration in **2**.

the weight loss of 15.17% between 20 °C and 220 °C represented elimination of the water and DMF molecules of crystallization (15.28% loss calcd). For **2**, the weight loss of 4.45% up to 180 °C corresponds to the removal of water molecules (cacld 4.84%). No further weight loss is observed between 180 °C and 320 °C, and decomposition begins at 320 °C. For **3**, dehydration occurred between 20 °C and 120 °C, as indicated by a total weight loss of 11.89% (cacld 11.91%). Rapid elimination of the organic

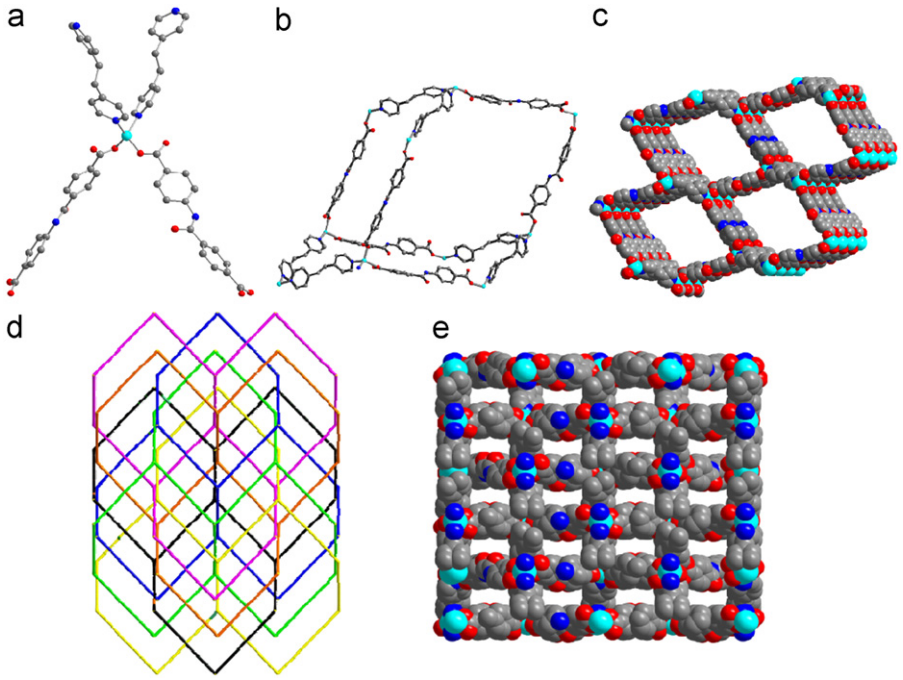

Fig. 3. Crystal structure of $[ZnL(bpa)]\cdot 4H_2O$ **3**: (a) coordination environment around Zn^{II} in **3**; (b) single diamondoid cage in **3**; (c) a single 3D framework of **3**; (d) schematic diagram of the 6-fold interpenetration in **3**; (e) space-filling showing of the 1D rectangle channels in **3** after 6-fold interpenetration.

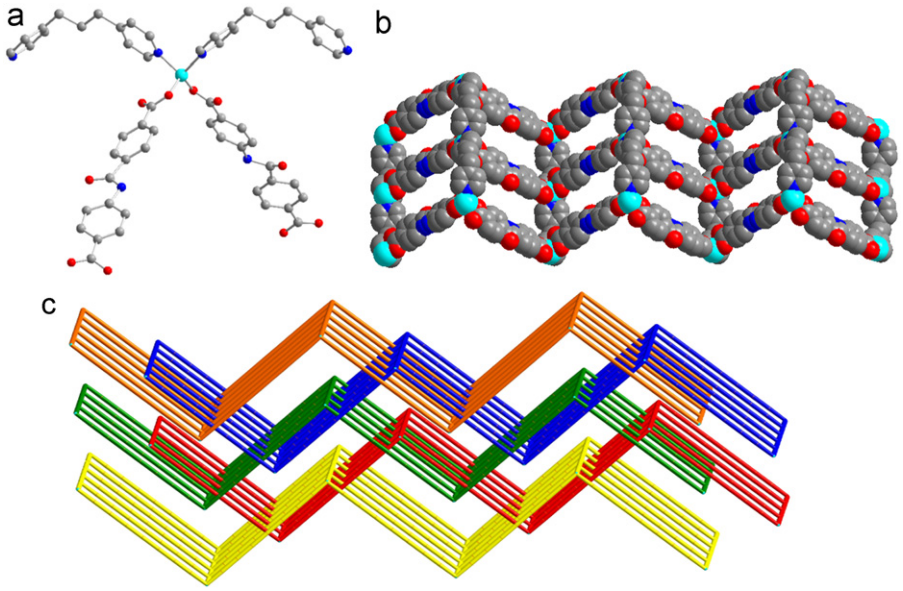

Fig. 4. Crystal structure of $[ZnL(bpp)]\cdot 1.75H_2O$ **4**: (a) coordination environment of Zn^{II} in **4**; (b) corrugated layer structure of **4**; (c) schematic illustration of the parallel polycatenation in **4**.

components occurred above 300 °C. For **4**, expulsion of the water molecules happened in the range of 25 °C and 100 °C (obsd 5.62%, cacld 5.45%), the mass remained largely stable until 380 °C.

PXRD analyses are carried out to check the structural identity. For **1–4**, the measured PXRD pattern closely matches the one simulated from single-crystal diffraction data, indicating the phase purity (Figs. S5–S8).

3.5. Photoluminescent properties

Photoluminescent properties of metal-containing complexes have attracted much attention due to their potential applications in electroluminescent display, chemical sensors, and photochemistry [16]. The luminescent properties of complexes **1–4** as well as the free H_2L ligand were investigated in the solid state at room temperature. Complexes **1** and **4** exhibit very weak fluorescent emission under experimental conditions, whereas **2** and **3** exhibit emission enhancement (Fig. 5).

The main emission peak of the free H_2L at 433 nm (λ_{ex}=334 nm) may be ascribed to the $\pi*\rightarrow\pi$ or $\pi*\rightarrow n$ transitions [17]. Complexes **2**, **3** show emission peaks at 464 nm (λ_{ex}=365 nm) and 453 nm (λ_{ex}=320 nm), respectively. The enhancement of luminescence for the two complexes compared with the free H_2L under the same conditions may mainly originate from coordination of the ligand to a $zinc^{II}$ ion, which effectively increases the rigidity of the ligand and reduces thermal

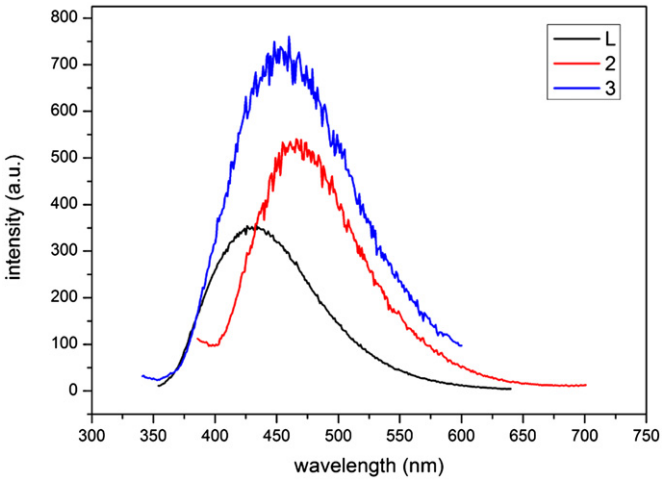

Fig. 5. Solid-state photoluminescence spectra of H_2L, complexes **2** and **3**.

vibrations, thereby reducing the nonradiative decay of the intraligand [18]. Besides, in comparison with the free ligand, red-shifts of about 31 nm and 20 nm are found for **2** and **3**, respectively, which may result from ligand-to-metal charge transfer (LMCT) [19]. The results suggest that design structure of the MOFs by incorporation of the exo-bidentate bipyridine ligands is a promising strategy to synthesize novel materials with unique photoluminescent properties.

4. Conclusion

In summary, the incorporation of linear spacers as bridges into the Zn–H_2L system under solvothermal conditions has yielded four new complexes **1**–**4** exhibiting a topological evolution from 3-fold interpenetration to 6-fold interpenetration and 2D→3D parallel polycatenation. Complex **1** has a triply interpenetrated pillared three-dimensional framework, whereas complexes **2** and **3** each features diamondoid network with 6-fold interpenetration. It is of particular interest to point out that the porosity of **3** is 25.8% despite 6-fold interpenetration, which is much higher than that of **2** (15.8%). Further increase of the length and flexibility of the bipyridine ligand to bpp gave rise to **4**, which display an interesting entangled architecture of 2D→3D parallel polycatenation. The results indicate that these structures are greatly affected by the spacer ligands. Though the generation of these interpenetrating structures is unpredictable, the results provide some clues to rationally design and synthesize novel interpenetrating architectures, which may shed some light on the design and synthesis of MOFs with novel structures. Further research on rational design and construction of a series of tunable microporous MOFs for application in gas storage and photoluminescence is currently underway.

Acknowledgments

This work was supported by the National Natural Science Foundation of China (NSFC No. 20801018), Shanghai education development foundation for financial support (Grant No. 2008CG31) and Shanghai Rising-Star Program (10QA1402000).

References

[1] (a) H.H. Wu, Q.H. Gong, D.H. Olson, J. Li, Chem. Rev. 112 (2012) 836;
(b) K. Sumida, D.L. Rogow, J.A. Mason, T.M. McDonald, E.D. Bloch, Z.R. Herm, T.H. Bae, J.R. Long, Chem. Rev. 112 (2012) 724;
(c) J.R. Li, J. Sculley, H.C. Zhou, Chem. Rev. 112 (2012) 869;
(d) M. Yoon, R. Srirambalaji, K. Kim, Chem. Rev. 112 (2012) 1196.
[2] (a) J. Kim, S.T. Yang, S.B. Choi, J. Sim, J. Kim, W.S. Ahn, J. Mater. Chem. 21 (2011) 3070;
(b) O.K. Farha, C.D. Malliakas, M.G. Kanatzidis, J.T. Hupp, J. Am. Chem. Soc. 132 (2010) 950;
(c) Q. Li, W. Zhang, O.Š. Miljanić, C.B. Knobler, J.F. Stoddart, O.M. Yaghi, Chem. Commun. 46 (2010) 380.
[3] B.L. Ivanov, M.S. Wellons, C.M. Lukehart, J. Am. Chem. Soc. 131 (2009) 11744.
[4] S.C. Xiang, X.T. Wu, J.J. Zhang, R.B. Fu, S.M. Hu, X.D. Zhang, J. Am. Chem. Soc. 127 (2005) 16352.
[5] K. Sumida, C.M. Brown, Z.R. Herm, S. Chavan, S. Bordiga, J.R. Long, Chem. Commun. 47 (2011) 1157.
[6] (a) Z. Fang, Y.F. Liu, Y.T. Fan, Y.H. Ni, X.W. Wei, K.B. Tang, J.M. Shen, Y. Chen, J. Phys. Chem. C 115 (2011) 13968;
(b) L.Q. Ma, W.B. Lin, J. Am. Chem. Soc. 130 (2008) 13834;
(c) P. Pachfule, R. Das, P. Poddar, R. Banerjee, Inorg. Chem. 50 (2011) 3855.
[7] (a) Z. Chang, D.S. Zhang, Q. Chen, R.F. Li, T.L. Hu, X.H. Bu, Inorg. Chem. 50 (2011) 7555;
(b) L.F. Ma, L.Y. Wang, Y.Y. Wang, S.R. Batten, J.G. Wang, Inorg. Chem. 48 (2009) 915.
[8] (a) H.H. Wu, R.S. Reali, D.A. Smith, M.C. Trachtenberg, J. Li, Chem. Eur. J. 16 (2010) 13951;
(b) A. Lan, K.H. Li, H.H. Wu, L.Z. Kong, N. Nijem, D.H. Olson, T.J. Emge, Y.J. Chabal, D.C. Langreth, M.C. Hong, J. Li, Inorg. Chem. 48 (2009) 7165;
(c) J.M. Zhang, H.H. Wu, T.J. Emge, J. Li, Chem. Commun. 46 (2012) 9152;
(d) A.J. Lan, K.H. Li, H.H. Wu, D.H. Olson, T.J. Emge, W. Ki, M.C. Hong, J. Li, Angew. Chem. Int. Ed. 48 (2009) 2334.
[9] S. Hasegawa, S. Horike, R. Matsuda, S. Furukawa, K. Mochizuki, Y. Kinoshita, S. Kitagawa, J. Am. Chem. Soc. 129 (2007) 2607.
[10] (a) M. Deniz, J. Pasan, J. Ferrando-Soria, O. Fabelo, et al., Inorg. Chem. 50 (2011) 10765;
(b) T.K. Maji, K. Uemura, H. Chang, R. Matsuda, S. Kitagawa, Angew. Chem. Int. Ed. 43 (2004) 3269;
(c) D. Sarma, K.V. Ramanujachary, S.E. Lofland, T. Magdaleno, S. Natarajan, Inorg. Chem. 48 (2009) 11660.
[11] P. Cavalleri, N.N. Chavan, A. Ciferri, C. DellErba, A.E. Lozano, M. Novi, J. Preston, Macromolecules 30 (1997) 3112.
[12] Y.Q. Sun, J. Hu, H.H. Zhang, Y.P. Chen, J. Solid State Chem. 186 (2012) 189.
[13] (a) G.M. Sheldrick, SHELXS-97, Program for Crystal Structure Solution, Göttingen University, Germany, 1997;
(b) G.M. Sheldrick, SHELXL-97, Program for Crystal Structure Refinement, Göttingen University, Germany, 1997.
[14] A.L. Spek, J. Appl. Crystallogr. 36 (2003) 7.
[15] (a) X.X. Xu, X. Zhang, X.X. Liu, L.S. Wang, E.B. Wang, Cryst. Eng. Commun. 14 (2012) 3264;
(b) B. Xu, Z.J. Lin, L.W. Han, R. Cao, Cryst. Eng. Commun. 13 (2011) 440.
[16] (a) M.S. Wang, S.P. Guo, Y. Li, L.Z. Cai, J.P. Zou, G. Xu, W.W. Zhou, F.K. Zheng, G.C. Guo, J. Am. Chem. Soc. 131 (2009) 13572;
(b) S. Barman, J.A. Garg, O. Blacque, K. Venkatesan, H. Berke, Chem. Commun. 48 (2012) 11127;
(c) C.A. Allen, S.M. Cohen, J. Mater. Chem. 22 (2012) 10188.
[17] Y.J. Cui, Y.F. Yue, G.D. Qian, B.L. Chen, Chem. Rev. 112 (2012) 1126.
[18] (a) S. Pramanik, C. Zheng, X. Zhang, T.J. Emge, J. Li, J. Am. Chem. Soc. 133 (2011) 4153;
(b) M.D. Allendorf, C.A. Bauer, R.K. Bhakta, R.J.T. Houk, Chem. Soc. Rev. 38 (2009) 1330;
(c) J. Zhao, X.L. Wang, X. Shi, Q.H. Yang, C. Li, Cryst. Growth Des. 11 (2011) 1531.
[19] (a) X.L. Chen, L. Gou, H.M. Hu, F. Fu, Z.X. Han, H.M. Shu, M.L. Yang, G.L. Xue, C.Q. Du, Eur. J. Inorg. Chem. 2 (2008) 239;
(b) Q. Chu, G.X. Liu, Y.Q. Huang, X.F. Wang, W.Y. Sun, Dalton Trans. 38 (2007) 4302;
(c) L.Y. Zhang, G.F. Liu, S.L. Zheng, B.H. Ye, X.M. Zhang, X.M. Chen, Eur. J. Inorg. Chem. 19 (2003) 2965.